Hydraulic determination of dam releases to generate warning waves in a mountain stream: performance of an analytical kinematic wave model

Frédéric Stilmant, University of Liege (ULg), Research Group of Hydraulics in Environmental and Civil Engineering (HECE), Allée de la Découverte 9, B-4000 Liège, Belgium (corresponding author). Email: frederic_stilmant@yahoo.fr

Michel Pirotton, Professor, University of Liege (ULg), Research Group of Hydraulics in Environmental and Civil Engineering (HECE)

Pierre Archambeau, Research Associate, University of Liege (ULg), Research Group of Hydraulics in Environmental and Civil Engineering (HECE)

Sébastien Erpicum, Research Associate, University of Liege (ULg), Research Group of Hydraulics in Environmental and Civil Engineering (HECE)

Benjamin Dewals, Associate Professor, University of Liege (ULg), Research Group of Hydraulics in Environmental and Civil Engineering (HECE)

Abstract

In this case study, we study the generation of warning waves with prescribed characteristics in a mountain stream. We determine which dam release will generate the desired warning wave. We solve this inverse problem following a two-model approach. An analytical kinematic model is used for a preliminary design of the dam release and a detailed two-dimensional (2D) fully dynamic model is used to converge to the final solution. Although the presented case study is far from an idealized academic case, the analytical model performs well and, beyond its role for preliminary design, turns out to be of prime interest for both understanding and discussing the results of the detailed 2D

model. The complex interactions between the release hydrograph, the geometry of the river and the friction formula are brought to light by the analytical model, which highlights the complementarity of both models and the usefulness of such a two-model approach.

Keywords

Warning wave; Inverse problem; Analytical model

Introduction

The operation of many hydropower schemes is based on the derivation of water from a river, through a penstock or a gallery, to the hydropower plant. Such schemes involve a water intake structure located upstream, often associated with a small dam, as well as a downstream outlet structure located typically several kilometers downstream (Fig. 1). In the river reach located between the upstream water intake and the downstream outlet structure (referred hereafter as the *bypassed* reach), the flow rates are much lower than they were before the construction of the hydropower scheme. However, under particular circumstances (malfunctioning of the hydropower plant or evacuation of excess flood discharge from upstream), it may be necessary to suddenly release a substantially higher discharge in this river reach. This sudden increase in discharge may cause danger for various users of this river reach, particularly in the case of recreational activities (e.g. fishing, bathing, hiking). One possible measure for mitigating this risk is the design of a warning system to alert users of the bypassed reach of the imminent danger.

One non-structural option for this consists in controlled releases of the upstream dam to generate a so-called *warning wave* along the bypassed reach. Such a wave must be designed such as to provide a clear signal of danger to the users of the river but it must not be dangerous. Thus the amplitude of this wave (in terms of variations in water depths and velocities) and its steepness (time interval over which the final amplitude of the wave is reached) must comply with a number of requirements all along the bypassed reach. The actual features of the warning wave however depend on the combined effect of the controlled release at the upstream dam and the properties of the river reach such as slope, cross-sectional shape and roughness; they are the solution of a so-called signaling problem (Whitham, 1974). As a result, determining the dam release which results in a warning wave with predefined properties implies the resolution of an *inverse* signaling problem (Sellier 2016): which boundary conditions lead to a wave that meets the requirements during its subsequent propagation?

Inverse problems look for the causes leading to known consequences, or for a model's parameters for known outputs. They are present in many engineering fields but are often ill-posed, i.e. the existence, uniqueness and/or stability of their solution is not guaranteed (Sabatier 2000; Sellier 2016). The standard formulation for an inverse problem is the search for the minimum of an objective function. Several optimization methods can thus be used as solution strategies (see Gunzburger (2003) and Sellier (2016) for a review in the field of free surface hydraulics). These methods are iterative and require generally many runs of the direct model, which may become computationally intractable when detailed multidimensional (2D, 3D) flow models are used.

In this context, simplified analytical models have an advantage over complex numerical models for posing the problem and helping to converge to the solution. Several authors combined analytical and detailed flow models for the study of wave propagations in rivers, particularly in the case of flow induced by dam break or debris flow (e.g. Aureli et al. 2014; Pudasaini et al. 2011). Experience shows that a preliminary design based on a simplified model provides valuable information on the underlying physics and on the range of solutions (existence conditions, identification of over-constrained problem…) which may be overlooked if only a complex numerical model is used. This latter model however plays also a part in that it helps refining the solution by accounting for details neglected in the simplified model.

In this paper, we present a case study in which the inverse problem of the determination of a dam release to generate a warning wave is solved based on a two-model approach. An analytical kinematic model is used for a preliminary design of the dam release and a detailed 2D fully dynamic model is used to converge to the final solution. The strength of this combination is particularly obvious in the sensitivity analysis conducted for the final solution, where the simplified model provides a clear understanding of an a priori surprising behavior of the solution.

The two-model approach is presented based on a case study in a mountain stream, which is described in section 2. The hydraulic models are depicted in section 3, while the results are discussed in section 4.

Case study

Context

We consider as a case study a hydropower scheme under construction in the French Alps, on the river Romanche, in the municipality of Livet-et-Gavet. The project, called 'Romanche Gavet' and carried out by Electricité de France (EDF), consists in the replacement of five one-century-old hydropower schemes by a single larger one.

The new scheme consists in (Fig. 1) an upstream water intake, nearby a 4.7m-high and 40m-wide upstream dam, a tunnel, as well as a downstream hydropower plant, nearby a 6m-high and 40m-wide downstream dam. The hydropower plant is equipped with two Francis turbines, working under a head of 270m and a total discharge of $41m^3/s$.

In this study, the focus is set on the river reach located between the upstream and downstream dams (bypassed reach). It is approximately 9.5km long and has a mean slope of about 3% (Fig. 2); the width of the main riverbed is approximately 30m. Topographic data, obtained from high resolution laser altimetry were available on a 1m × 1m Cartesian grid. This high resolution grid is valuable here to reproduce the highly irregular riverbed (see the many changes in flow regime induced by these irregularities as exemplified in the detail of Fig. 1).

Under normal operation of the new hydropower scheme, the discharge flowing through the bypassed reach is maintained at a low value of $4m^3/s$ (environmental flow). In case of a malfunctioning of the hydropower plant or in case of the arrival of a flood wave, the river reach is used to evacuate the excess discharge from upstream towards downstream, which may imply a sudden and large increase of the discharge in the bypassed reach.

Warning wave

The dam operator must trigger a so-called warning wave in the downstream reach before releasing high discharges. The features of this warning wave were defined based on considerations on the vulnerability associated to different usages of the downstream river reach (recreational, fishing, bathing, hiking…). The determination of these features of the warning wave lies out of the scope of the present study, which is dedicated to the calculation of the upstream dam release (Fig. 3) suitable to produce the desired warning wave features in the bypassed river reach (Fig. 4).

In the present case, the warning wave consists in a relatively rapid increase in water depth and flow velocity. It corresponds to a prescribed rise in discharge from its initial value Q_0 up to a predefined discharge Q_p. The warning wave must additionally fulfil the following criteria:

- The dynamics of the wave must be such that the water level increases as fast as possible but with a gradient that remains below an upper bound called $G_{\max}$ in order to prevent any danger for the users of the river. On a limnigraph, this gradient is defined between the beginning of the increase in water level and up to the time when 80% of the total increase in water level is reached (Fig. 4a).
- All along the bypassed reach, the maximum discharge of the warning wave must be kept during a minimum time interval $\Delta t_{\min}$ before any further increase in discharge. In practice, this time interval is defined as the time during which the discharge remains between $Q_p^- = Q_p$ - 1m³/s and $Q_p^+ = Q_p$ + 1m³/s (Fig. 4b).

In the present case study, the following parameter values were used: Q_0 = 4m³/s, Q_p = 10m³/s, $G_{\max}$ = 8cm/min (1.33×10^{-3}m³/s), $\Delta t_{\min}$ = 60s. This set of values defines a so-called “reference scenario”, while the effect of varying these values is analyzed in section Discussion in which alternate release scenarios are considered.

The objective of this study is to design a release hydrograph at the upstream dam so that all the above requirements are fulfilled all along the bypassed river reach. The two degrees of freedom to achieve this are the rising time ΔT_1 and the duration of the plateau ΔT_2 (Fig. 3).

Hydraulic models

Detailed 2D model

Detailed 2D flow simulations were performed using Wolf2D, an academic code developed at the University of Liege (Belgium). It solves the conservative form of the 2D shallow-water equations (Guinot 2008; Wu 2008) on multiblock Cartesian grids based on a finite volume scheme. A flux vector splitting method is used to handle shocks and flow regime transitions accurately (Erpicum et al. 2010a). The time integration is performed by means of an explicit Runge-Kutta algorithm. The model was validated in previous studies, both against field data (Erpicum et al. 2010b) and experimental observations of complex turbulent flow (Peltier et al. 2015; Roger et al. 2009).

The computation domain covers the bypassed river reach, between the upstream dam (near the water intake) and slightly downstream of the outlet of the hydropower plant, where another dam is located. The downstream boundary condition is a constant free surface elevation, consistently with the operation rules of the downstream dam. The upstream boundary condition is the hydrograph to be determined. The characteristics of the detailed 2D model are given in Tab. 1.

Friction modelling

The size of the particles covering the riverbed ranges from a few centimeters to several decimeters, i.e. a value which is similar to the water depth. For this reason, we did not use a standard formula for friction modelling, such as Manning formula, but instead we opted for the physically-based Barr-Bathurst formula as proposed by Machiels et al. (2011).

The friction coefficient λ (-) in Darcy-Weisbach's formulation depends on the relative roughness k_s/h, where k_s (m) is the characteristic size of the roughness elements and h (m) the water depth. For relatively small values of k_s, λ also depends on the Reynolds number. For relatively large values of k_s (i.e. $k_s/h \geq 0.15$), λ is given by:

$$\frac{1}{\lambda^{1/2}} = -1.987 \log\left[\frac{1}{5.15}\min\left(\frac{k_s}{h},1\right)\right] \tag{1}$$

When the characteristic size of the roughness k_s exceeds the water depth h, the friction coefficient λ reaches a maximum value of 0.5 and becomes independent of the size of the roughness elements.

Formulation (1) leads to discontinuous expressions for the wave celerity of a kinematic model and its derivatives (see Eqs. (20) and (21)). However, this formulation is necessary to account for the macro-rough flow conditions in the river. Particularly, it reflects the distinct influence of the characteristic height k_s of roughness elements depending on whether the water depth is higher or lower than k_s.

The model was calibrated against measured free surface elevations obtained from a field survey conducted by EDF in 2011. A total of 3,130 point measurements were collected in six different areas of the considered river reach. Based on these field data, the characteristic size of the roughness has been set to a constant value of 0.4m, except in the most upstream part of the river (zone A-B in Figs. 1-2), where it has been set to 0.15m, consistently with the milder slope and the finer bed material in this area (Tab. 1).

Analytical model

Applicability

The fully dynamic shallow-water equations may be reasonably approximated by different simplified models depending on the value of non-dimensional numbers, mainly the kinematic wave number *k* and the Froude number *F*, defined as:

$$k = \frac{g S_0 A^2 L}{Q^2}, \qquad F = \frac{Q}{A(gh)^{1/2}} \tag{2}$$

with S_0 (-) the mean slope of the river reach, *A* (m²) its mean cross-section, *L* (m) its length, *Q* (m³/s) the discharge, *h* (m) the typical water depth and *g* (m/s²) the gravity acceleration.

In the present case study, the following values may be considered: $S_0 \sim 0.03$, $L \sim 10$km, $h \sim 0.3$m, $A \sim 10$m², $Q \sim 10$m³/s. Hence, typical values of *k* and *F* are, respectively: $k \sim 3 \times 10^3$ and $F \sim 0.5$, which indicates that a kinematic wave approximation is applicable, since $k >> 1$ (Singh 2001; Sturm 2010).

Model derivation

Under this approximation, the flow discharge is simply deduced from a friction formula and the governing equations reduce to a single partial differential equation expressing mass conservation (Whitham, 1974; Hunt, 1984a; Hunt, 1984b), with *t* (s) the time and *x* (m) the abscissa in the streamwise direction:

$$\frac{\partial A}{\partial t} + \frac{\partial Q}{\partial x} = 0 \tag{3}$$

Different friction formulas can be used provided that the discharge *Q* is continuously differentiable with respect to the cross-section *A*. We assume a friction formula in which the discharge Q depends only on the cross-section A, i.e. parameters like the friction coefficient or the wetted parameter can vary with A, but the purely geometrical parameters of the river, like its slope or its width, are constant in space and time:

$$Q = Q(A) \tag{4}$$

The characteristic form of Eq. (3) reads

$$\frac{\mathrm{d}A}{\mathrm{d}t} = 0 \tag{5}$$

and is valid along space-time paths (the characteristic curves), defined by the following wave celerity:

$$c = \frac{\mathrm{d}x}{\mathrm{d}t} = \frac{\mathrm{d}Q}{\mathrm{d}A} \tag{6}$$

Eq. (5) states that, along these paths, the flow properties (i.e. A, but also Q according to Eq. (4)) remain constant. As a result, these characteristic curves are straight lines.

In the space-time plane (x, t), the characteristic curves originating from the initial condition (locus defined by $x > 0$, $t = 0$) and the characteristic curves originating from the boundary condition (locus defined by $x = 0$, $t > 0$) define the flow properties in the whole domain (i.e. for $x > 0$ and $t > 0$). However, depending on the flow conditions, characteristic curves can merge, which generates a shock, i.e. a discontinuity in the flow as the flow properties are not unique at these points.

To further study the conditions under which shocks appear, it is necessary to specify some properties of the function $Q(A)$: for $A \geq 0$, $Q(A)$ and its first two derivatives are positive. These properties are shared by numerous friction formulas.

As the celerity given by (6) increases with A and therefore with Q, an upstream boundary condition corresponding to a rising hydrograph is likely to lead to a shock (Fig. 5). Following a procedure applied by Capart (2013) in the case of a dam breaching on an initially dry bed, we derive the position of the wave front under the assumption that the shock occurs at this front. We then verify under which condition this is actually the case (Appendix 2). The initial condition is a steady flow with a discharge Q_0 and a cross section A_0. The upstream boundary condition is a hydrograph $Q(0, t) = Q_R(t)$ characterizing the dam release. Subscript 'R' ('Release') is also used for the other parameters directly related to the upstream boundary condition, i.e. the upstream cross section $A_R = A(Q_R)$ and the corresponding wave celerity $c_R = c(Q_R)$.

The position of the front (x_F, t_F) is given by the integration of the continuity equation (3) on the domain Ω defined in Fig. 5 and the application of Green-Gauss' theorem:

$$0 = \iint_\Omega \left(\frac{\partial A}{\partial t} + \frac{\partial Q}{\partial x} \right) \mathrm{d}\Omega = \int_\Gamma Q\,\mathrm{d}t - A\,\mathrm{d}x \tag{7}$$

where $\Gamma = \Gamma_1 \cup \Gamma_2 \cup \Gamma_3 \cup \Gamma_4$ is the contour of the domain Ω, oriented anticlockwise. In the following, parameter τ (s) is a time measured at the upstream boundary condition.

Taking advantage of Q and A being constant on Γ_2, Γ_3 and Γ_4, this leads to:

$$\underbrace{-\int_0^\tau Q_R(t)\,\mathrm{d}t}_{\Gamma_1} \underbrace{-A_0 x_F}_{\Gamma_2} \underbrace{+Q_0 t_F}_{\Gamma_3} \underbrace{-Q_R(\tau)(t_F - \tau) + A_R(\tau)\,x_F}_{\Gamma_4} = 0 \tag{8}$$

Or, after rearrangement:

$$-\int_0^\tau [Q_R(t) - Q_0]\,\mathrm{d}t - [Q_R(\tau) - Q_0](t_F - \tau) + [A_R(\tau) - A_0]\,x_F = 0 \tag{9}$$

Since the characteristic curve originating from $(0, \tau)$ is a straight line, we have:

$$x_F = c_R(\tau)(t_F - \tau) \tag{10}$$

Substituting Eq. (10) into Eq. (9) gives:

$$t_F = \tau + \frac{\int_0^\tau [Q_R(t) - Q_0]\,\mathrm{d}t}{c_R(\tau)[A_R(\tau) - A_0] - [Q_R(\tau) - Q_0]}, \tag{11}$$

$$x_F = c_R(\tau) \frac{\int_0^\tau [Q_R(t) - Q_0]\,\mathrm{d}t}{c_R(\tau)[A_R(\tau) - A_0] - [Q_R(\tau) - Q_0]} \tag{12}$$

The denominator in Eqs. (11) and (12) is greater or equal to 0 for $A_R(\tau) \geq A_0$ because the function $Q(A)$ is convex as it is twice piecewise differentiable and has a positive second derivative (Boyd et al., 2009). However, expressions (11) and (12) do not tend to the origin of the axes as τ tends to 0. Under the assumption of continuous functions, they instead respectively tend to (see Appendix 1):

$$t_{F,0} = \lim_{\tau \to 0} t_F = \frac{c_0}{\left.\frac{\mathrm{d}c_R}{\mathrm{d}Q}\right|_{Q=Q_0} \left.\frac{\mathrm{d}Q_R}{\mathrm{d}t}\right|_{t=0}} \tag{13}$$

$$x_{F,0} = \lim_{\tau \to 0} x_F = \frac{c_0^2}{\left.\frac{\mathrm{d}c_R}{\mathrm{d}Q}\right|_{Q=Q_0} \left.\frac{\mathrm{d}Q_R}{\mathrm{d}t}\right|_{t=0}} \tag{14}$$

Thus, from (0, 0) to ($x_{F,0}$, $t_{F,0}$), the wave front follows the characteristic curve originating from (0, 0). At ($x_{F,0}$, $t_{F,0}$), the first shock occurs and the wave front then follows the path given by (11) and (12). Its propagation velocity is given by:

$$v_F = \frac{\mathrm{d}x_F}{\mathrm{d}t_F} = \frac{\frac{\mathrm{d}x_F}{\mathrm{d}\tau}}{\frac{\mathrm{d}t_F}{\mathrm{d}\tau}} = \frac{Q_R(\tau) - Q_0}{A_R(\tau) - A_0} \tag{15}$$

which is Rankine-Hugoniot's formula. From Eq. (15), it is clear that if the upstream hydrograph reaches a constant value, the velocity of the propagation of the wave front finally becomes constant. The path of the wave front then becomes a straight line again.

Note that, if $\mathrm{d}Q_R/\mathrm{d}t = 0$ for $t = 0$, $t_{F,0}$ and $x_{F,0}$ as given by (13) and (14) are both infinite. This however does not necessarily exclude the presence of a shock as discussed below.

The above developments have been made under the assumption that, if a shock appears, the shock is located at the wave front and not upstream of it (otherwise, the upper edge of the domain Ω in Fig. 5 would not be a straight line). As detailed in Appendix 2, this is indeed the case for linear hydrographs and hydrographs rising less than proportionally to time, and for usual friction formulae such as Eq. (1).

Application to the case study

To apply the model to the case study, the upstream boundary condition and the considered friction formula must be specified. The former corresponds to the dam release, which is composed of two successive linear hydrographs. The slopes of this hydrograph are denoted by γ (m^3/s^2):

$$\frac{\mathrm{d}Q_R}{\mathrm{d}t} = \gamma \tag{16}$$

Thus, for $\tau \leq \Delta T_1 + \Delta T_2$, we have (the developments for $\tau > \Delta T_1 + \Delta T_2$ are equivalent):

$$\begin{gathered} \tau \leq \Delta T_1 \Rightarrow \int_0^\tau \left[Q_R(t) - Q_0 \right] \mathrm{d}t = \frac{\gamma \tau^2}{2} \\ \Delta T_1 < \tau \leq \Delta T_1 + \Delta T_2 \Rightarrow \int_0^\tau \left[Q_R(t) - Q_0 \right] \mathrm{d}t = \gamma \Delta T_1 \left(\tau - \frac{1}{2} \Delta T_1 \right) \end{gathered} \tag{17}$$

Besides, we use the Bathurst friction formula (1) (the full expression of the Barr-Bathurst formula is not necessary given the low water depths) in combination with a Darcy-Weisbach formulation, i.e. the discharge Q can be evaluated by:

$$Q = \left(\frac{8 g S_0 A^3}{P \lambda} \right)^{1/2} \tag{18}$$

The friction coefficient λ (-) is a function of A, through the water depth h, which we assume to be approximated by A/b where b is the width of the river. The wetted perimeter P (m) is also a function of A. However, since the water depth h ~ 0.3m is about two orders of magnitude smaller than the width b ~ 30m of the river, the wetted perimeter P is well approximated by the width and is therefore considered as a constant. Thus, after grouping all constant parameters in a coefficient α (s^{-1}), Eq. (18) can be rewritten as (with 'log' the base 10 logarithm and 'ln' the natural logarithm):

$$\begin{cases} Q = 1.987 \log(5.15) \alpha A^{3/2} & \text{if } A \le b k_s \\ Q = 1.987 \log\left(5.15 \dfrac{A}{b k_s}\right) \alpha A^{3/2} & \text{if } b k_s < A < \dfrac{b k_s}{0.15} \end{cases}, \qquad \alpha = \left(\frac{8 g S_0}{b} \right)^{1/2} \tag{19}$$

The celerity (6) is then given by:

$$\begin{cases} c = \dfrac{3}{2} 1.987 \log(5.15) \alpha A^{1/2} & \text{if } A \le b k_s \\ c = \dfrac{3}{2} 1.987 \left[\log\left(5.15 \dfrac{A}{b k_s}\right) + \dfrac{2}{3} \dfrac{1}{\ln 10} \right] \alpha A^{1/2} & \text{if } b k_s < A < \dfrac{b k_s}{0.15} \end{cases} \tag{20}$$

And the derivative of the celerity reads:

$$\begin{cases} \dfrac{\mathrm{d}c}{\mathrm{d}Q} = \dfrac{1}{2A} & \text{if } A \le b k_s \\ \dfrac{\mathrm{d}c}{\mathrm{d}Q} = \dfrac{1}{2A} \dfrac{\log\left(5.15 \dfrac{A}{b k_s}\right) + \dfrac{8}{3} \dfrac{1}{\ln 10}}{\log\left(5.15 \dfrac{A}{b k_s}\right) + \dfrac{2}{3} \dfrac{1}{\ln 10}} & \text{if } b k_s < A < \dfrac{b k_s}{0.15} \end{cases} \tag{21}$$

Note that neither c nor dc/dQ are continuous at $A = bk_s$. These discontinuities are not negligible since they represent respectively 41 % of c and 87 % of (dc/dQ) for $A = bk_s$. However, on both sides of the discontinuity, the function $Q(A)$ and its first two derivatives are monotonic and $\mathrm{d}^3Q/\mathrm{d}A^3$ is negative, so that, according to Appendix 2, the analytical model can be applied on both sides of the discontinuity in expression (20) for the wave celerity.

The values of two parameters have to be specified: k_s and b. The characteristic size of the roughness elements k_s was set to 0.4m during the calibration of the detailed 2D model. The fact that k_s was set to 0.15m in the most upstream part of the river (zone A-B in Fig. 1) is disregarded here because the analytical model assumes constant parameters along the river. The mean width b of the river was estimated at 30m (surface of the flow divided by the curvilinear length of the river). Thus, with a mean slope of $S_0 = 0.03$, the coefficient α defined by (19) takes a value of $0.28\mathrm{s}^{-1}$.

The cross-section for which the expressions of Q, c and dc/dQ change is $A_s = bk_s = 12\mathrm{m}^2$. The corresponding discharge is $Q_s = 16\mathrm{m}^3/\mathrm{s}$, i.e. the change does not occur in the warning wave, but in the wave generated by the subsequent release. This second release is almost a shock, so that the discontinuity in the friction formula does not affect the results. In the warning wave, the friction coefficient λ is constant and equal to its maximal value.

Further approximation

As shown in Fig. 6, the path of the front of the warning wave is successively described by a straight line from (0, 0) to ($x_{F,0}$, $t_{F,0}$), a non-linear curve from ($x_{F,0}$, $t_{F,0}$) to ($x_{F,p}$, $t_{F,p}$) and a straight line beyond ($x_{F,p}$, $t_{F,p}$). For a preliminary design, it can be useful to replace the non-linear part by a straight line, the slope of which is given by:

$$v_{F,m} = \frac{x_{F,p} - x_{F,0}}{t_{F,p} - t_{F,0}} = \frac{c_p \dfrac{1}{2} \dfrac{Q_p - Q_0}{c_p\left(A_p - A_0\right) - \left(Q_p - Q_0\right)} - \dfrac{c_0^2}{\left.\dfrac{\mathrm{d}c}{\mathrm{d}Q}\right|_0 \left(Q_p - Q_0\right)}}{1 + \dfrac{1}{2} \dfrac{Q_p - Q_0}{c_p\left(A_p - A_0\right) - \left(Q_p - Q_0\right)} - \dfrac{c_0}{\left.\dfrac{\mathrm{d}c}{\mathrm{d}Q}\right|_0 \left(Q_p - Q_0\right)}} \qquad (22)$$

This value is independent of the rising time ΔT_1. Hereafter, the results based on the linearization of the front trajectory are referred to as *approximate* results (subscript 'approx').

Results

Two parameters of the release at the upstream dam have to be determined (Fig. 3):

- The rising time, ΔT_1, which must be such that the gradient of the limnigraphs does not exceed G_{max} (Fig. 4a);
- The duration of the plateau, ΔT_2, which must be such that the time interval during which the hydrograph remains between Q_p^- and Q_p^+ is not lower than Δt_{min} = 60s (Fig. 4b).

The constraints associated with both parameters can be interpreted as minimum time intervals between the occurrence of two successive values in the limnigraphs or in the hydrographs (Fig. 4). The analytical model predicts that, in the case of increasing discharges, all time intervals decrease with the distance to the upstream dam (Fig. 7a) because the celerity c given by (20) increases with Q. Thus, the determining river section for the design of the wave is the most downstream one.

In the following, the results ΔT_1 and ΔT_2 obtained with the analytical model are presented and compared to those of the detailed 2D model. The results of the latter model are given as multiples of 60s (i.e. there was no attempt to get results with a finer precision).

Rising time

According to the analytical model, when the discharge rises from Q_0 = 4m³/s to Q_p = 10m³/s, the water depth rises from h_0 = 0.16m to h_p = 0.29m. Hence, the water depths in the bypassed reach are roughly doubled by the warning wave. The average increase in flow velocity is around 40 %. The water depth required for the computation of the water level gradient is $h_{80\%}$ = 0.26m, which corresponds to a discharge $Q_{80\%}$ = 8.7m³/s and a celerity $c_{80\%}$ = 1.66m/s. At the upstream dam, this discharge is released at $t_{80\%} = (Q_{80\%} - Q_0)/(Q_p - Q_0)\,\Delta T_1 = 0.78\Delta T_1$. Downstream of the bypassed reach, the minimum time interval between h_0 and $h_{80\%}$ so that the maximum value of the gradient $G_{\max}$ is verified is $t_{\min} = (h_{80\%} - h_0)/G_{\max}$ = 79s (Fig. 4a).

According to (22), $v_{F,m}$ = 1.41m/s in the approximated analytical model. The minimum duration of the rising time at the upstream dam can be deduced from the path of the front and the characteristic line originating at $t_{80\%}$, together with (14). It is given by:

$$\Delta T_{1,\text{approx}} = \frac{t_{\min} + \dfrac{L}{v_{F,m}} - \dfrac{L}{c_{80\%}}}{\dfrac{Q_{80\%} - Q_0}{Q_p - Q_0} + \dfrac{2A_0 c_0}{Q_p - Q_0}\left(\dfrac{c_0}{v_{F,m}} - 1\right)} = 1823\text{s} \tag{23}$$

The complete analytical model (solution of a non-linear equation) leads to ΔT_1 = 1979s. The detailed 2D model (iterative procedure) gives ΔT_1 = 1920s. The results of both models are given in Tab. 2 and plotted in Fig. 7.

The results of the detailed 2D model presented in Fig. 7 correspond to points located in the center of the river, taken every 50m. For all positions, the limnigraphs have been processed so as to find h_0, t_0, $h_{80\%}$ and $t_{80\%}$ (as defined in Fig. 4a). Fig. 7b (detailed 2D) shows that the changes in water depth induced by the warning wave along the bypassed reach have a large dispersion: the standard deviation $\sigma_{\Delta h}$ = 0.035m is equal to 28% of the mean value $\mu_{\Delta h}$ = 0.13m. In contrast, Fig. 7a and c show that the times at which t_0 and $t_{80\%}$ are reached display a clear trend. Thus, the irregularities of the riverbed have a direct impact on the local amplitude of the warning wave while their impacts on the propagation velocity of the warning wave are more or less compensated. In the end, as shown in Fig. 7d, the gradient $\Delta h/\Delta t$ of the warning wave still displays a clear steepening of the wave as predicted by the analytical model: $\Delta h/\Delta t$ increases by one order of magnitude from upstream to downstream.

The results of the analytical model compare surprisingly well with those of the detailed 2D model despite the broad range of flow features which are not explicitly taken into account by the analytical model. In the analytical model, the idealization of the topography (Fig. 2) does not only reduce all water depths to a single value for a given discharge (Fig. 7b) but it also overlooks the numerous changes in flow regime (critical sections and hydraulic jumps) which are present along the bypassed reach according to the detailed 2D model (Fig. 1). Nonetheless, the fact that both intermediate results (amplitude and arrival time of the warning wave) are well reproduced demonstrates the valuable contribution of the analytical model for the preliminary design of the warning release.

Nevertheless, differences between both models remain. First, the downstream boundary condition (constant water depth at the downstream dam) is not taken into account in the analytical model. Its influence on the results of the detailed 2D model can be seen clearly in Fig. 7d: the maximum value of the gradient of the warning wave is not situated at the very end of the bypassed reach but several hundred meters upstream because the amplitude of the wave is cancelled out at the downstream dam by the boundary condition and is attenuated in its vicinity due to the backwater effect. Another difference between the results of both models is induced by diffusion. Upstream of the bypassed reach, a 600m-long zone has a slope which is significantly lower than the mean value of 3% (zone A-B in Fig. 1). In this zone, the kinematic number k is much lower and the kinematic theory is not strictly applicable. Therefore, the arrival times t_0 and $t_{80\%}$ as given by the detailed 2D model in Fig. 7a are delayed.

Duration of the plateau

The minimum time interval between the arrival of the discharges $Q_p^- = 9\text{m}^3/\text{s}$ and $Q_p^+ = 11\text{m}^3/\text{s}$ at a given location must be higher than $\Delta t_{\min} = 60\text{s}$ (Fig. 4b). According to the analytical model, the determining section is again the most downstream one. The discharge Q_p^- belongs to the warning wave and, since the rising time ΔT_1 has already been set ($\Delta T_1 = 1920\text{s}$), its arrival time at $x = L$ is known (according to (12), the characteristic curve originating from $(0, \tau_p^-)$ does not intersect the front within the computation domain): $t_p^- = 7240\text{s}$ (rounded to a multiple of 60s). As a result, the arrival time of the discharge Q_p^+ at $x = L$ must be $t_p^+ = t_p^- + 60 = 7300\text{s}$. The discharge Q_p^+ belongs to the second release and, since the steepness of this second release is much higher than the one of the warning release ($\Delta Q = 68\ \text{m}^3/\text{s}$ in $\Delta t = 60\text{s}$), it is reasonable to consider that all characteristic curves merge before $x = L$. Indeed, according to (11) and (12), with $\tau = 60\text{s}$, all characteristic curves have merged 360m downstream of the upstream dam and 120s after the release of the second wave. The front then propagates at a velocity given by Eq. (15):

$$v_F = \frac{Q_f - Q_p}{A_f - A_p} = \frac{78-10}{26.1-8.6} = 3.88\text{m/s} \qquad (24)$$

This leads to:

$$\Delta T_2 = t_p^+ - \frac{L-360}{v_F} - 120 - \Delta T_1 = 2900s \qquad (25)$$

The detailed 2D model (iterative procedure) gives ΔT_2 = 2700s. The results of both models are given in Tab. 2 and plotted in Fig. 8a. The differences are twofold. First, for the path of Q_p^-, the propagation velocity given by the detailed 2D model for the first 600m is lower than the value given by the analytical model. As already stated in the previous subsection, this is due to the milder slope in this zone which induces a diffusion of the wave. Second, for the path of Q_p^+, the propagation velocities given by both models differ along the whole bypassed reach. The origin of this difference is also a diffusion phenomenon, which can be understood based on the hydrographs displayed in Fig. 8b. Since the second release at the upstream dam is much steeper than the warning release, the diffusion, which is proportional to the second derivative of Q with respect to x, is also much higher. At x = 600m, the shape of the hydrograph corresponding to the second release has been modified in such a way that it is no longer linear (in contrast to what happens for the warning release). For x > 600m, the hydrograph steepens, but, as can be deduced from (11) and (12), it has acquired a shape which is much less conducive to a full steepening than the linear shape. As a result, at x = 9000m, the shock has only developed for the first half part of the hydrograph. Thus, using Q_f = 78m³/s in Eq. (24) leads to an important overestimation of the celerity of the front of the second release.

Discussion

The results discussed so far were obtained by assuming that the model parameters (such as k_s) and the constraints on the warning wave (Q_p, Q_f, $\Delta t_{\min}$) take the same value as used in the real-world case study. This is referred to as a “reference scenario”. Here, we analyse how the results are affected when different values are considered for the roughness height k_s, the discharge Q_p of the warning wave, the discharge Q_f of the second wave, and the minimum time $\Delta t_{\min}$ between the warning wave and the second wave.

We highlighted above that expressions (20) and (21) for the wave celerity and its first derivative are discontinuous for $A = bk_s$. For the values of the parameters considered in the real-world case study (reference scenario), this discontinuity has no consequence on the results ΔT_1 and ΔT_2 because it only affects the second wave. Here, to enable exploring a wider range of values for parameters k_s, Q_p and Q_f, we first fix this issue of a discontinuous expression for the wave celerity. To do so, we slightly adapt the analytical model so that all expressions become continuous. We also show that this adaptation of the model hardly changes the model results for the reference scenario.

In the following, we first introduce the upgraded analytical model. Then, we discuss the influence of the roughness height k_s on the model results and, finally, we test three alternate designs of the warning wave.

Continuous analytical model

The function $Q(A)$ given by Eq. (19) can be rewritten as:

$$Q = 1.987 \log\left[5.15 f(A)\right] \alpha A^{3/2}, \qquad f(A) = \max\left(1,\ \frac{A}{bk_s}\right) \tag{26}$$

The function $f(A)$ is not continuously differentiable for $A = bk_s$. It can however be approximated by the following expression, which is continuously differentiable:

$$f(A)=\left[1+\left(\frac{A}{bk_s}\right)^{\beta}\right]^{1/\beta}, \tag{27}$$

with β a dimensionless parameter ($\beta \in$]1; +∞[). Eq. (27) tends towards the 'max'-function as in Eq. (26) when $\beta \to +\infty$.

With this expression, Eqs. (20)-(21) become:

$$c=\frac{3}{2}1.987\left\{\log\left[5.15 f(A)\right]+\frac{2}{3}\frac{1}{\ln 10}\left[\frac{1}{f(A)}\frac{A}{bk_s}\right]^{\beta}\right\}\alpha A^{1/2} \tag{28}$$

$$\frac{\mathrm{d}c}{\mathrm{d}Q}=\frac{1}{2A}\frac{\log\left[5.15 f(A)\right]+\frac{8}{3}\frac{1}{\ln 10}\left[\frac{1}{f(A)}\frac{A}{bk_s}\right]^{\beta}\left[1+\frac{1}{2}\frac{\beta}{f(A)^{\beta}}\right]}{\log\left[5.15 f(A)\right]+\frac{2}{3}\frac{1}{\ln 10}\left[\frac{1}{f(A)}\frac{A}{bk_s}\right]^{\beta}} \tag{29}$$

For $\beta < 8$, the conditions detailed in Appendix 2 are met for all discharges, so that the smoothed analytical model can be applied in any configuration. Note that given the high irregularity of the riverbed, a smoothing of the friction formula makes sense from a physical point of view: not all points of a given cross section reach a water depth $h = k_s$ at the same time.

The results of this continuous model are given in Tab. 3 and compared to the results obtained previously. The smoothing of the friction formula induces changes in ΔT_1 and ΔT_2 which remain below 180s. The results of the continuous analytical model differ from those of the detailed 2D model by less than 240s. Therefore, all results of the analytical model presented hereafter are obtained with the smoothed friction formula.

Sensitivity to roughness

The values of rising time ΔT_1 and duration of the plateau ΔT_2 presented above are based on the value k_s = 0.4m which was calibrated so as to reproduce available data with the detailed 2D model. As an uncertainty is still associated with this parameter, we analyzed the effect of this parameter on the results obtained above. According to the analytical model, k_s has a direct impact on the celerity of the characteristic curves and, thus, on the time intervals which have been computed.

The sensitivity analysis presented below shows how the maximum gradient of the warning wave induced by the release defined above is influenced by the value of k_s. The results of both models (detailed 2D model and continuous analytical model) are given in Fig. 9. Both models display a behavior which is not monotonic. They both highlight a maximum in the value of the gradient when the uncertain parameter k_s is varied.

This behavior is surprising at first sight but can be easily understood thanks to the analytical model. For low k_s values, the friction coefficient in Bathurst formula (19) depends on k_s and is an increasing function of this parameter (case $bk_s < A$). Thus, an increase in k_s leads to an increase in the water depths, Eq. (19). As the increase is higher for higher water depths, there is an increase in the amplitude of the wave (in terms of water depths). Besides, an increase in k_s leads to a decrease in the wave celerities, Eq. (20). As the decrease is lower for higher water depths, there is a decrease in the time interval $t_{80\%} – t_0$. Both effects result in a steepening of the warning wave.

Above a certain value of k_s, the water depth in the initial condition becomes lower than k_s. As a result, the initial condition (A_0, h_0, c_0) becomes independent of the value of k_s. The amplitude of the warning wave thus increases even more, but the time interval $t_{80\%} – t_0$ starts increasing, which leads to a decrease of the wave steepness after passing a maximum (infinite in this case because the characteristic curve originating from $t_{80\%}$ intersects the front before $x = L$ and thus leads to a shock).

For a second value of k_s, the water depth for Q_p also becomes lower than k_s. As a result, the whole warning wave becomes independent of k_s.

In the results of the detailed 2D model, there are two main differences. First, the diffusion that appears for high gradients smoothens the steepness of the wave. Second, the irregularity of the riverbed leads to a high dispersion of the water depths within a given cross section, so that the threshold effects are not as distinctive as in the analytical model results (not all water depths in a cross section are lower or higher than k_s).

Alternate release scenarios

The characteristics of the warning wave (such as Q_p and $\Delta t_{\min}$) should be related to safety criteria for the people to be alerted. The stability of people partly immerged in water is commonly assessed based on the product of the flow velocity and the water depth (Martinez et al. 2016). Accepted thresholds for this product are around 0.4m²/s for children and 0.6m²/s for adults (AR&R guidelines, Cox et al. 2010). The comparison of these criteria with the function $Q(A)$ of the analytical model shows that the warning wave in the reference scenario is safe for children (Fig. 10).

Here, we tested an alternate design of the warning wave, in which safety is ensured for adults but not for children. This corresponds to Q_p = 16m³/s. As shown in Tab. 4, the rising time ΔT_1 increases by +90% (which is larger than the increase in Q_p +60%) compared to the reference scenario. The comparison between the continuous analytical model and the detailed 2D model (differences are less than 240s) further confirms the validity of the analytical model.

The influence of the minimum time interval $\Delta t_{\min}$ on the value of ΔT_2 is straightforward in the analytical model: since the warning wave has no influence on the second wave and vice-versa, any increase in $\Delta t_{\min}$ results in the same increase in ΔT_2. This behavior is also observed in the detailed 2D model.

We also tested alternate release scenarios, in which the amplitude Q_f of the second wave is higher than in the case study. As it may correspond for instance to a flood release scenario, we set the value of Q_f to the annual flood discharge Q_f = 150m³/s. The time interval ΔT_1 is not affected. Tab. 5 shows how the value of ΔT_2 changes when Q_p and Q_f are varied. Compared to the reference scenario, a substantial increase in Q_f (+92%) results in a comparatively low increase in ΔT_2 (+18%). Moreover, an increase in Q_p decreases the value of ΔT_2. In all these scenarios, the differences between the continuous analytical model and the detailed 2D model are again less than 240s.

Conclusion

In this paper, we have presented a case study in which the inverse problem of the determination of a dam release to generate a predefined warning wave in a mountain stream is solved based on a two-model approach. The derivation of an analytical kinematic model has been justified based on dimensionless numbers that characterize the flow. This analytical model succeeds in summarizing the wealth of information provided by a detailed 2D fully dynamic model and leads to results which do not only display and explain the main trends in the behavior of the flow but also give correct orders of magnitudes. In particular, the comparison between the analytical model and the detailed 2D model highlights the effect of the irregularities in the riverbed, the change in slope, the shape of the hydrograph and the characteristic size of the roughness of the riverbed. These insights are of valuable importance for a deep understanding of the flow process and for confirming the relevance of the results obtained from detailed flow simulations.

The analytical kinematic model has been derived (Eqs. (11) to (15)) so as to accommodate more general release hydrographs and other friction models than those analyzed in the presented case study. As a result, the analytical model can also apply to other configurations in which an input hydrograph requires optimization with respect to downstream flow characteristics (warning waves, sediment flushing …).

Appendices

Derivation of the space-time coordinates at which the shock first develops ($x_{F,0}$, $t_{F,0}$)

The expression of $t_{F,0}$ in Eq. (13) is obtained as follows. Both the numerator and denominator of Eq. (11) tend to 0 for τ tending to 0. The indetermination is solved thanks to l'Hospital's theorem, which applies for continuous functions:

$$\begin{aligned} t_{F,0} &= \lim_{\tau\to 0} \frac{\int_0^\tau [Q_R(t)-Q_0]\,\mathrm{d}t}{c_R(\tau)[A_R(\tau)-A_0]-[Q_R(\tau)-Q_0]} \\ &= \lim_{\tau\to 0} \frac{\dfrac{\mathrm{d}}{\mathrm{d}\tau}\left\{\int_0^\tau [Q_R(t)-Q_0]\,\mathrm{d}t\right\}}{\dfrac{\mathrm{d}}{\mathrm{d}\tau}\{c_R(\tau)[A_R(\tau)-A_0]-[Q_R(\tau)-Q_0]\}} \\ &= \lim_{\tau\to 0} \frac{Q_R(\tau)-Q_0}{\dfrac{\mathrm{d}}{\mathrm{d}\tau}[c_R(\tau)][A_R(\tau)-A_0]+c_R(\tau)\dfrac{\mathrm{d}}{\mathrm{d}\tau}[A_R(\tau)]-\dfrac{\mathrm{d}}{\mathrm{d}\tau}[Q_R(\tau)]} \\ &= \lim_{\tau\to 0} \frac{1}{\dfrac{\mathrm{d}}{\mathrm{d}\tau}[c_R(\tau)]}\frac{Q_R(\tau)-Q_0}{A_R(\tau)-A_0} \end{aligned} \tag{30}$$

The last line in Eq. (30) is obtained from the following relation:

$$\frac{\mathrm{d}Q}{\mathrm{d}\tau} = \frac{\mathrm{d}Q}{\mathrm{d}A}\frac{\mathrm{d}A}{\mathrm{d}\tau} = c\frac{\mathrm{d}A}{\mathrm{d}\tau} \tag{31}$$

The result in Eq. (30) contains also an indetermination, which is again solved thanks to l'Hospital's theorem and Eq. (31):

$$\lim_{\tau\to 0}\frac{Q_R(\tau)-Q_0}{A_R(\tau)-A_0}=\lim_{\tau\to 0}\frac{\dfrac{\mathrm{d}}{\mathrm{d}\tau}\left[Q_R(\tau)-Q_0\right]}{\dfrac{\mathrm{d}}{\mathrm{d}\tau}\left[A_R(\tau)-A_0\right]}=\lim_{\tau\to 0}\frac{\dfrac{\mathrm{d}}{\mathrm{d}\tau}\left[Q_R(\tau)\right]}{\dfrac{\mathrm{d}}{\mathrm{d}\tau}\left[A_R(\tau)\right]}=\lim_{\tau\to 0}c_R(\tau) \qquad (32)$$

The combination of Eq. (30) and (32) gives Eq. (13).

The derivation of the expression of $x_{F,0}$ in Eq. (14) follows the same procedure as for the expression of $t_{F,0}$.

Condition under which a shock is located at the front of the wave

To establish the condition under which the assumption of Fig. 5 (i.e. a shock located at the front of the wave) applies, we derive the expression of the set of points at which two subsequent characteristic curves collide and compare them to the expressions of Eqs. (11) and (12). Let (x_C, t_C) be a point of the characteristic curve originating from (0, τ). The space and time coordinates x_C and t_C verify:

$$x_C=c_R(\tau)\left(t_C-\tau\right) \qquad (33)$$

If (x_C, t_C) corresponds to a shock, then this point can be reached by two neighbouring characteristic lines originating from x = 0 at two subsequent times, i.e. $\mathrm{d}x_C/\mathrm{d}\tau = \mathrm{d}t_C/\mathrm{d}\tau = 0$. The derivation of (33) with respect to τ then gives:

$$t_C=\tau+\frac{c_R(\tau)}{\left.\dfrac{\mathrm{d}c_R}{\mathrm{d}Q}\right|_{Q=Q_R(\tau)}\left.\dfrac{\mathrm{d}Q_R}{\mathrm{d}t}\right|_{t=\tau}} \qquad (34)$$

And, therefore:

$$x_C = \frac{c_R^2(\tau)}{\left.\frac{\mathrm{d}c_R}{\mathrm{d}Q}\right|_{Q=Q_R(\tau)} \left.\frac{\mathrm{d}Q_R}{\mathrm{d}t}\right|_{t=\tau}} \qquad (35)$$

For $\tau = 0$, (x_C, t_C) corresponds to $(x_{F,0}, t_{F,0})$, which further confirms that this point is the point at which a shock first develops. For $\tau > 0$, the assumption that no shock occurs behind the wave front holds as long as:

$$x_C(\tau) \geq x_F(\tau) \quad \Leftrightarrow \quad t_C(\tau) \geq t_F(\tau) \qquad (36)$$

According to (12) and (35), or, equivalently, to (11) and (34), this corresponds to:

$$\frac{\left.\frac{\mathrm{d}Q_R}{\mathrm{d}t}\right|_{t=\tau} \int_0^\tau [Q_R(t) - Q_0]\mathrm{d}t}{[Q_R(\tau) - Q_0]^2} \leq c_R(\tau) \frac{c_R(\tau)[A_R(\tau) - A_0] - [Q_R(\tau) - Q_0]}{[Q_R(\tau) - Q_0]^2 \left.\frac{\mathrm{d}c_R}{\mathrm{d}Q}\right|_{t=\tau}} \qquad (37)$$

For a given value of the parameter τ, the dimensionless value of the left-hand side only depends on the shape of the hydrograph which is prescribed as a boundary condition, i.e. on the shape of the function $Q_R(t)$. On the contrary, for a given value of τ, the right-hand side only depends on the shape of the friction formula which applies in the river, i.e. on the shape of the function $Q(A)$, since $A_R(\tau) = A[Q_R(\tau)]$, $c_R(\tau) = \mathrm{d}[Q_R(\tau)]/\mathrm{d}A$ and $(\mathrm{d}c_R/\mathrm{d}Q)_{t=\tau} = (\mathrm{d}c_R/\mathrm{d}Q)_{Q=QR(\tau)}$.

The right-hand side of Eq. (37) is positive because the function $Q(A)$ and its first two derivatives are positive. For A_τ tending to A_0, or, equivalently, for Q_τ tending to Q_0, we have, according to l'Hospital's theorem:

$$\lim_{A\to A_0}\frac{c(A-A_0)-(Q-Q_0)}{(Q-Q_0)^2}=\lim_{A\to A_0}\frac{\dfrac{\mathrm{d}}{\mathrm{d}A}\left[c(A-A_0)-(Q-Q_0)\right]}{\dfrac{\mathrm{d}}{\mathrm{d}A}\left[(Q-Q_0)^2\right]}=\lim_{A\to A_0}\frac{\dfrac{\mathrm{d}c}{\mathrm{d}A}(A-A_0)}{2(Q-Q_0)c}=\frac{1}{2c}\frac{\mathrm{d}c}{\mathrm{d}Q} \tag{38}$$

Thus, the right-hand side of Eq. (37) tends to 1/2 for A_τ tending to A_0, regardless of the function $Q(A)$. If the function $Q(A)$ and its first two derivatives are monotonic and if $\mathrm{d}^3Q/\mathrm{d}A^3$ is negative, then 1/2 is the minimum of the right-hand side of Eq. (37). Otherwise, the right-hand side may have another minimum for $A_\tau > A_0$, and the following conclusions would not necessarily apply for any value of A or Q.

For the left-hand side of Eq. (37), let $Q_R(t) - Q_0$ be a power law of the kind $Q_R(t) - Q_0 = \kappa\, t^n$. The left-hand side then equals $n/(n+1)$ and Eq. (37) reads:

$$\frac{n}{n+1}\le\frac{1}{2} \tag{39}$$

From Eq. (35), it is clear that a linear hydrograph ($n = 1$), as well as hydrographs rising less than proportionally to time ($n < 1$) fulfil the condition of a single shock located at the wave front. On the other hand, for hydrographs rising more than proportionally to time ($n > 1$), shocks can develop upstream of the wave front and influence its subsequent path.

Notation

The following variables are used in this paper:

$(\ldots)_0$ Variable in the initial state (A_0, c_0, h_0, Q_0)

$(\ldots)_{80\%}$ Variable in the state when 80% of the amplitude of the warning wave is reached ($A_{80\%}$, $c_{80\%}$, $h_{80\%}$, $Q_{80\%}$, $t_{80\%}$)

$(\ldots)_C$ Variable at a shock (t_C, x_C)

$(\ldots)_F$	Variable at the front of the warning wave (t_F, x_F)
$(\ldots)_{F,0}$	Variable at the front of the warning wave when the first shock occurs ($t_{F,0}$, $x_{F,0}$)
$(\ldots)_{F,p}$	Variable at the front of the warning wave when its path becomes linear ($t_{F,p}$, $x_{F,p}$)
$(\ldots)_{F,m}$	Mean value of a variable at the front of the warning wave along its nonlinear path ($v_{F,m}$)
$(\ldots)_f$	Variable in the final state (A_f, c_f, h_f, Q_f)
$(\ldots)_p$	Variable in the uniform flow established after the arrival of the warning wave (A_p, c_p, h_p, Q_p)
$(\ldots)_p^-$	Variable just before Q_p is reached (Q_p^-, t_p^-)
$(\ldots)_p^+$	Variable just after Q_p is left (Q_p^+, t_p^+)
$(\ldots)_R$	Variable at the upstream dam (A_R, c_R, h_R, Q_R)
$(\ldots)_s$	Value for which the 1D Barr-Bathurst formula is discontinuous (A_s, Q_s)
A	Cross-section
b	Section width
c	Wave celerity
F	Froude number
$G_{\max}$	Highest acceptable value for the gradient of the limnigraphs
g	Gravity acceleration
h	Water depth (h_p, h_0),
k	Kinematic wave number
k_s	Characteristic size of the roughness elements of the riverbed
L	Length of the bypassed reach
P	Wetted perimeter
Q	Discharge
S_0	Mean slope of the river

t	Time
n	Exponent
v	Propagation velocity of a discontinuity
x	Distance to the upstream dam
α	Coefficient in the 1D Barr-Bathurst formula
β	Coefficient in the smoothed Barr-Bathurst formula
Γ	Boundary of the integration domain which is used to derive the analytical model
γ	Slope of the hydrograph at the upstream dam
ΔT_1	Rising time of the warning wave at the upstream dam
ΔT_2	Duration of the plateau after the warning wave at the upstream dam
κ	Coefficient
λ	Friction coefficient
τ	Time
Ω	Integration domain which is used to derive the analytical model

Acknowledgement

The Authors gratefully acknowledge EDF for funding part of this research and for providing data.

References

Aureli, F., Maranzoni, A. and Mignosa, P. (2014). “A semi-analytical method for predicting the outflow hydrograph due to dam-break in natural valleys.” *Advances in Water Resources*, 63, 38–44.

Boyd, S. and Vandenberghe, L. (2009). *Convex optimisation*. University Press, Cambridge.

Capart, H. (2013). “Analytical solutions for gradual dam breaching and downstream river flooding.” *Water Resources Research*, 49, 1968–1987.

Cox, R. J., Shand, T. D., Blacka, M. J. (2010). “Australian Rainfall and Runoff (AR&R). Revision Project 10: Appropriate safety criteria for people. New South Wales, Australia.

Erpicum, S., Dewals, B., Archambeau, P. and Pirotton, M. (2010a). “Dam-break flow computation based on an efficient flux-vector splitting.” *Journal of Computational and Applied Mathematics*, 234, 2143–2151.

Erpicum, S., Dewals, B., Archambeau, P. and Pirotton, M. (2010b). “Detailed inundation modelling using high resolution DEMs.” *Engineering Applications of Computational Fluid Mechanics*.

Guinot, V. (2008). *Wave propagation in fluids: models and numerical techniques,* ISTE, London, U.K.

Gunzburger, M. D. (2003). *Perspectives in Flow Control and Optimization*. SIAM, Philadelphia.

Hunt, B. (1984a). “Dam-break solution.” *Journal of Hydraulic Engineering*, 110, 675-686.

Hunt, B. (1984b). “Perturbation solution for dam-break floods.” *Journal of Hydraulic Engineering*, 110, 1058-1071.

Machiels, O., Erpicum, S., Archambeau, P., Dewals, B. and Pirotton, M. (2011). “Theoretical and numerical analysis of the influence of the bottom friction formulation in free surface flow modelling.” *Water SA*, 37.

Martinez-Gomariz, E., Gomez, M., Russo, B. (2016). “Experimental study of the stability of pedestrians exposed to urban pluvial flooding” *Natural Hazards*, 82, 1259-1278.

Peltier, Y., Erpicum, S., Archambeau, P., Pirotton, M. and Dewals, B. (2015). “Can meandering flows in shallow rectangular reservoirs be modelled with the 2D shallow water equations?” *Journal of Hydraulic Engineering*, 141, 04015008.

Pudasaini, S. P. (2011). “Some exact solutions for debris and avalanche flows.” *Physics of fluids*, 23, 043301

Roger, S., Dewals, B., Erpicum, S., Schwanenberg, D., Schüttrumpf, H., Köngeter, J. and Pirotton, M. (2009). “Experimental and numerical investigations of dike-break induced flows.” *Journal of Hydraulic Research*, 47, 349–359.

Sabatier, P. C. (2000). “Past and future of inverse problems.” *Journal of Mathematical Physics*, 41, 4082–4124.

Sellier, M. (2016). “Inverse problems in free surface flows: a review.” *Acta Mechanica*, 227, 913–935.

Singh, V. P. (2001). “Kinematic wave modelling in water resources: a historical perspective.” *Hydrological Processes*, 15, 671–706.

Sturm, T. W. (2010). *Open Channel Hydraulics*. McGraw-Hill, New York.

Whitham, G. B. (1974). *Linear and nonlinear waves.* John Wiley & Sons, New York.

Wu, W. (2008). *Computational River Dynamics.* Taylor & Francis, London, U.K.

	Detailed 2D model	Analytical model
Hydraulic model	Dynamic wave	Kinematic wave
Friction formula	Barr-Bathurst	Barr-Bathurst
Dimensions	2D	1D
Slope	Distributed	Uniform value
Roughness	Reach A-B: k_s = 0.15m Reach B-C: k_s = 0.40m	k_s = 0.4m
Upstream boundary condition	Hydrograph	Hydrograph
Downstream boundary condition	Free surface level	None

Tab. 1. Characteristics of the two models.

	Analytical model		Detailed 2D model
	Approximate	Complete	
ΔT_1	1823s	1979s	1920s
ΔT_2		2900s	2700s

Tab. 2. Results given by the analytical model and the detailed 2D model. All values of ΔT_2 assume that ΔT_1 = 1920s.

Design result	Analytical model		Detailed 2D model
	Initial model	Continuous model	
ΔT_1	1979s	2120s	1920s
ΔT_2	2900s	2807s	2700s

Tab. 3. Comparison of the results given by the continuous model applied to the case study with the results obtained previously.

Scenario	Q_0	Q_p	Analytical model	Detailed 2D model
Reference scenario	4m³/s	10m³/s	2120s	1920s
Alternate scenario 1	4m³/s	16m³/s	3519s	3660s

Tab. 4. Computed values of ΔT_1 for different values of Q_p.

Scenario	Q_p	Q_f	Analytical model	Detailed 2D model
Reference scenario	10m³/s	78m³/s	2747s + Δt_{min}	2640s + Δt_{min}
Alternate scenario 1	16m³/s	78m³/s	1532s + Δt_{min}	1320s + Δt_{min}
Alternate scenario 2	10m³/s	150m³/s	3273s + Δt_{min}	3120s + Δt_{min}
Alternate scenario 3	16m³/s	150m³/s	1971s + Δt_{min}	1800s + Δt_{min}

Tab. 5. Computed values of ΔT_2 for different values of Q_p and Q_f.

Fig. 1. Sketch of the overall configuration in plane view (zoom: computed flow regime). Specific points are: A – upstream end; B – change in mean slope; C – downstream end.

Fig. 2. Streamwise profile of the riverbed along the river centerline. Specific points are: A – upstream end; B – change in mean slope; C – downstream end.

Fig. 3. Unknown parameters characterizing the release hydrograph at the upstream dam: ΔT_1 and ΔT_2.

Fig. 4. Time-constraints prescribed on the warning wave: (a) on the limnigraphs; (b) on the hydrographs. These constraints apply for all sections along the bypassed reach.

Fig. 5. Integration domain Ω for the definition of the position (x_F, t_F) of the wave front.

Fig. 6. (a) Hydrograph at the upstream boundary condition; (b) Resulting wave's front propagation along the river (–) and approximation (- -).

Fig. 7. Determination of the rising time of the release at the upstream dam based on the detailed 2D model (points) and the analytical model (lines): (a) paths of the front and the characteristic line associated with $h = h_{80\%}$ in the (x, t) plane; (b) change in water depth induced by the warning wave $\Delta h = h_{80\%} - h_0$; (c) time interval over which the change in water depth takes place $\Delta t = t_{80\%} - t_0$; (d) corresponding gradient. The square symbol in Fig. 7(a) represents the point where the kinematic wave front becomes a shock.

Fig. 8. Determination of the duration of the plateau of the release at the upstream dam: (a) paths of the discharges Q_p^- and Q_p^+ in the (x, t) plane based on the detailed 2D

model (points) and the analytical model (lines); (b) hydrographs at some locations as given by the detailed 2D model.

Fig. 9. Sensitivity of the maximum gradient of the warning wave with respect to the characteristic size of the roughness elements k_s.

Fig. 10. Comparison of the Barr-Bathurst formula with safety criteria for children and adults partly immerged in water (AR&R guidelines, Cox et al. 2010).

Figure 1 Click here to download Figure Graphique 1.tif

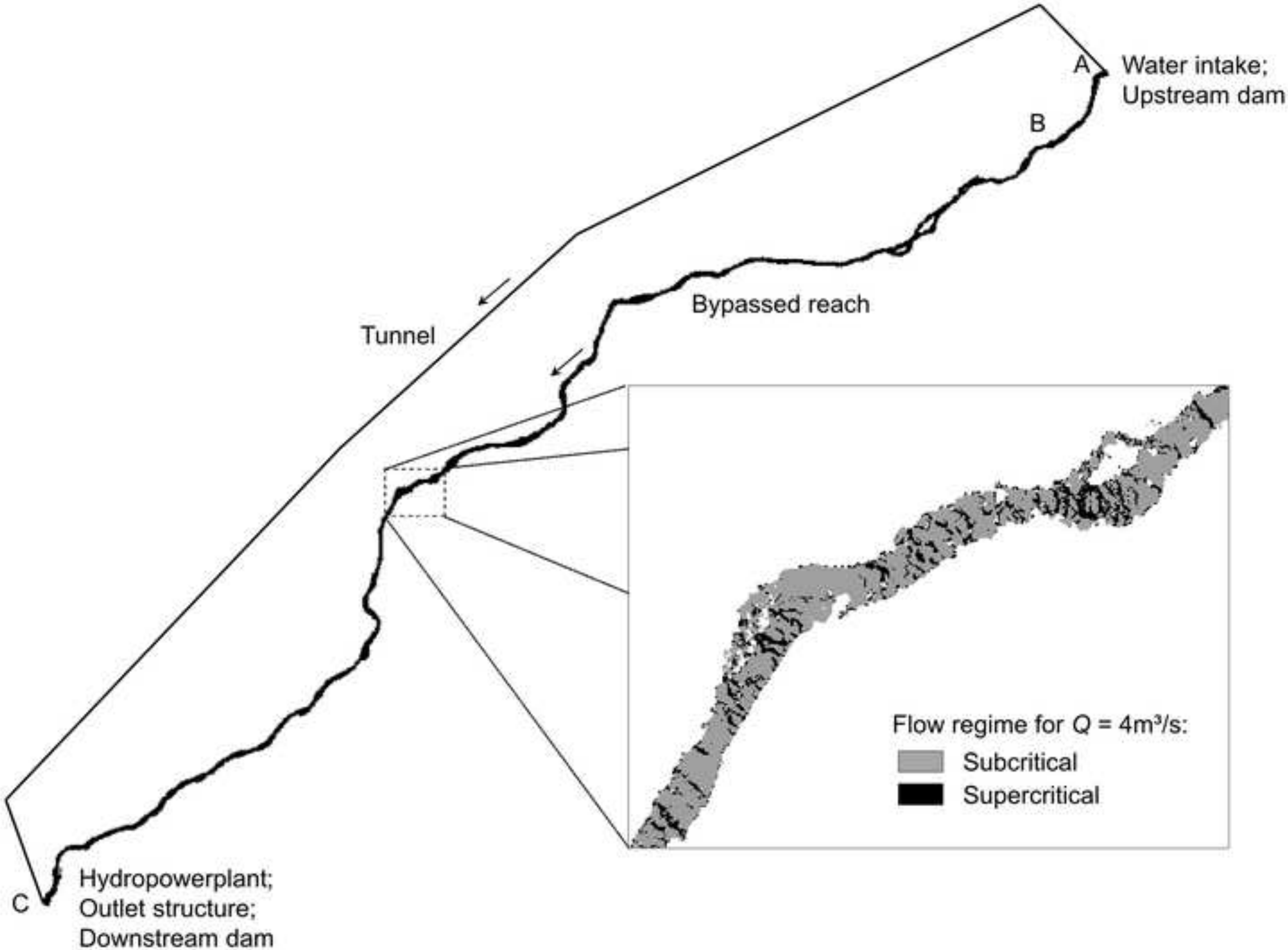

Figure 2

Click here to download Figure fig2.eps

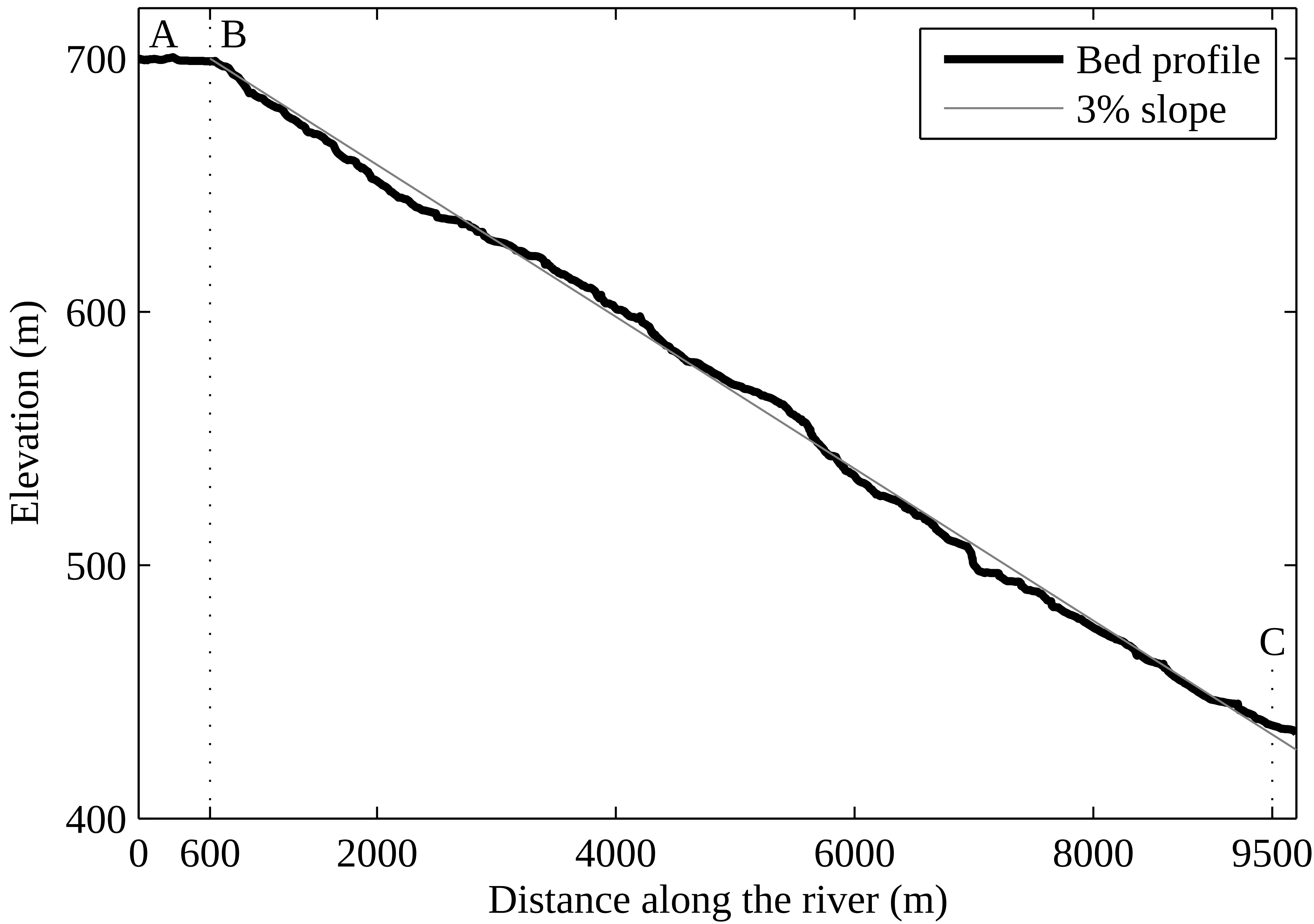

Figure 3

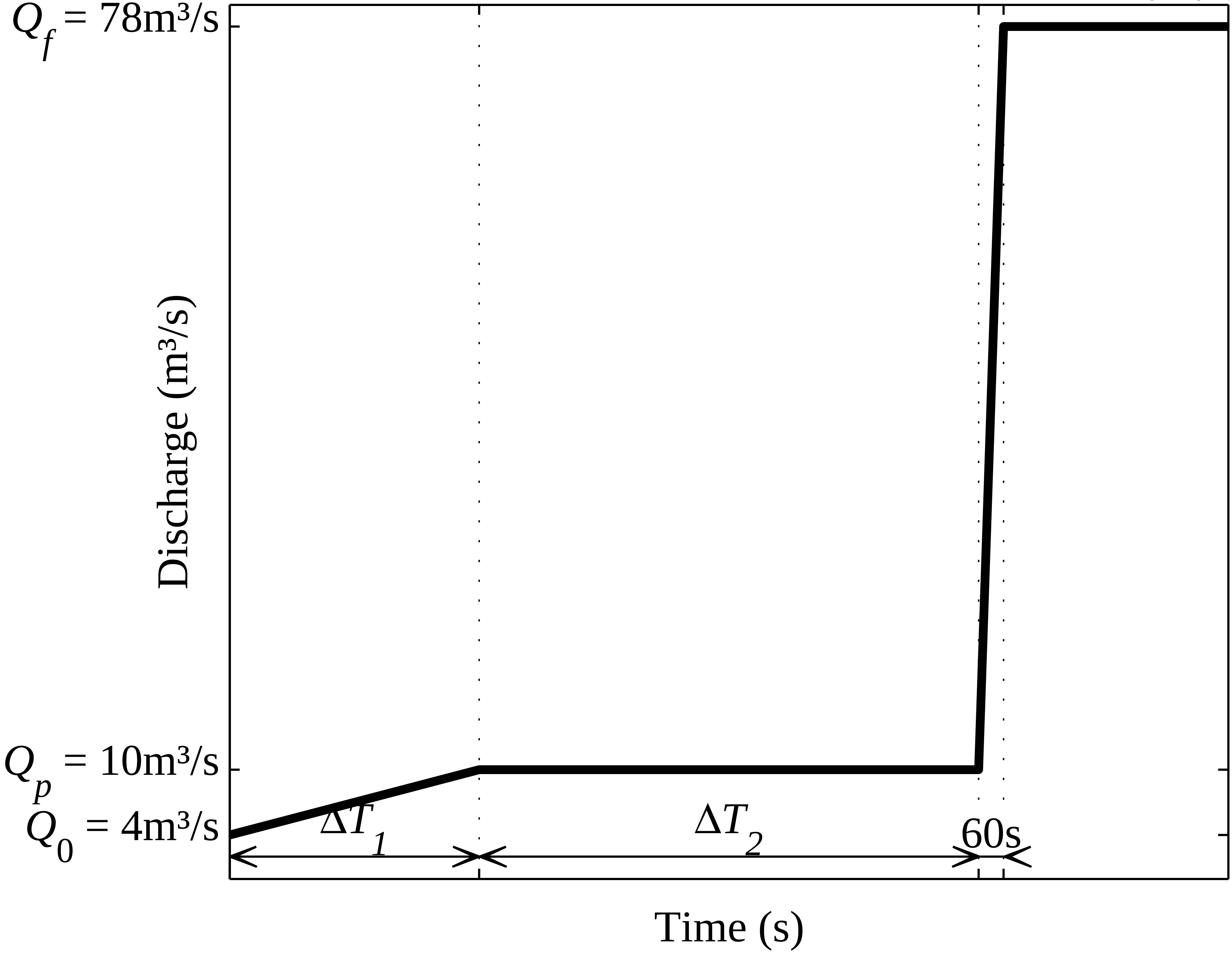
$Q_f = 78\text{m}^3/\text{s}$
$Q_p = 10\text{m}^3/\text{s}$
$Q_0 = 4\text{m}^3/\text{s}$
Discharge (m³/s)
ΔT_1
ΔT_2
60s
Time (s)

Figure 4

Click here to download Figure fig4.eps

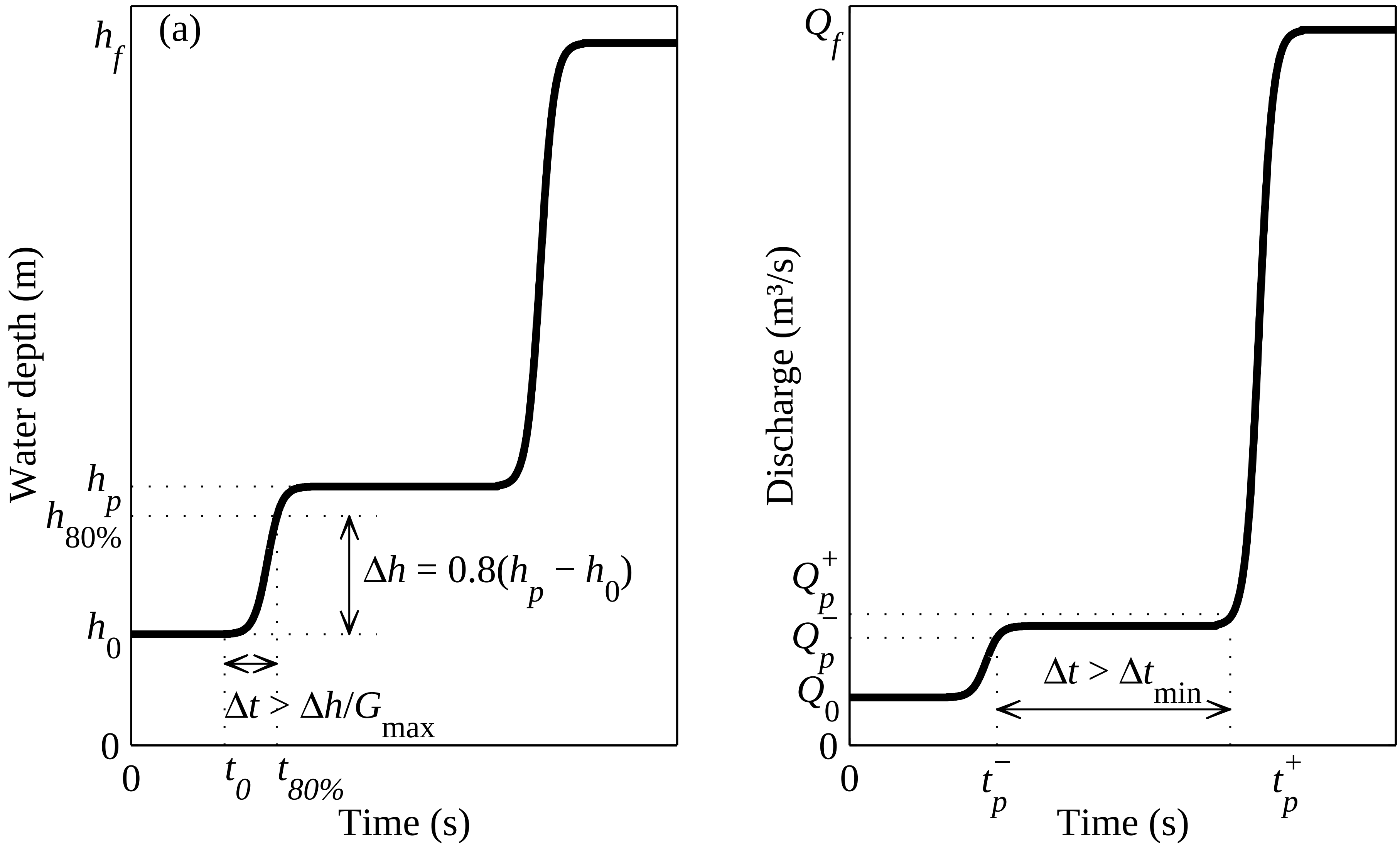

Figure 5

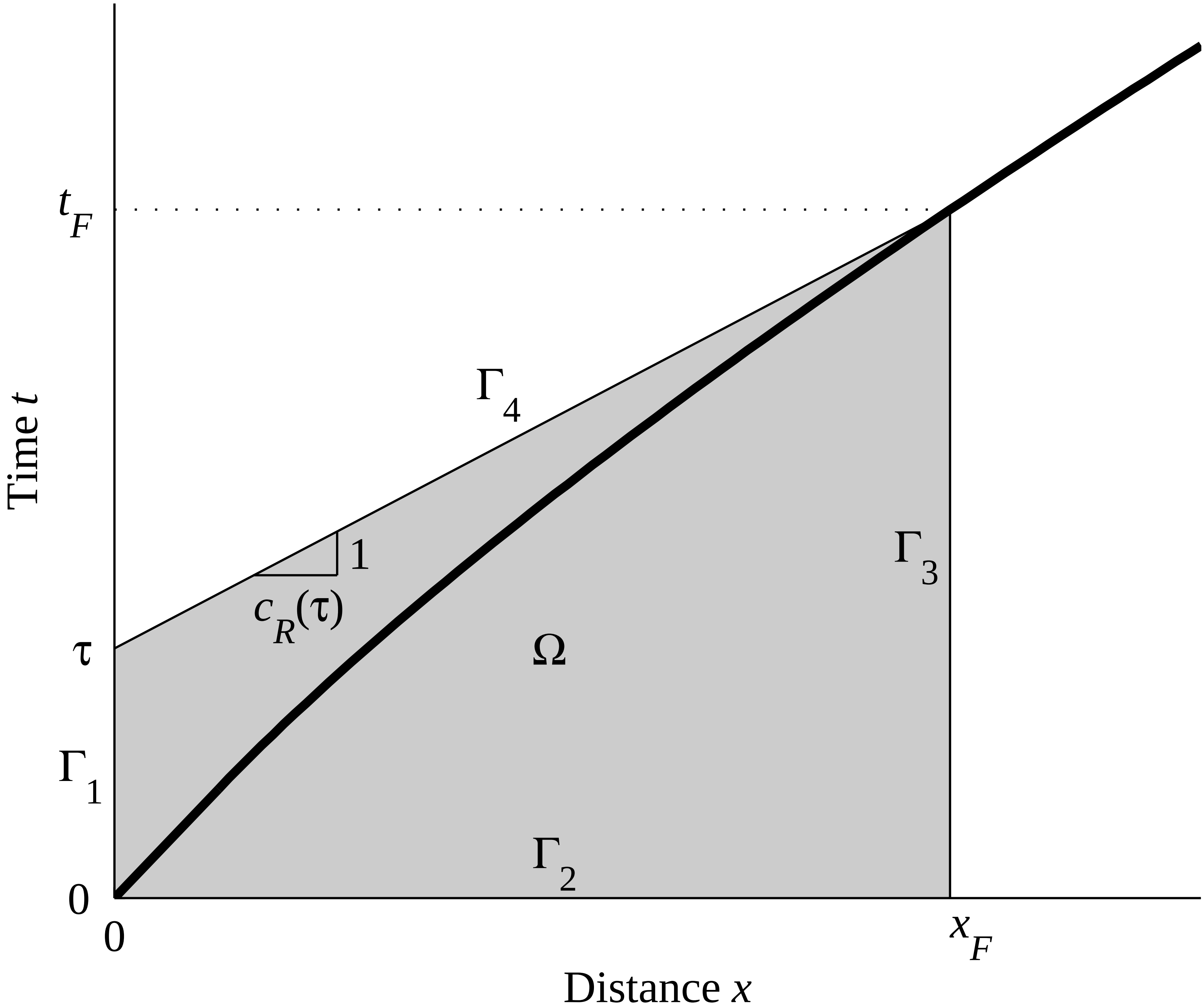

t_F
Time t
Γ_4
1
$c_R(\tau)$
τ
Γ_3
Ω
Γ_1
Γ_2
0
0
x_F
Distance x

Figure 6

Click here to download Figure fig6.eps

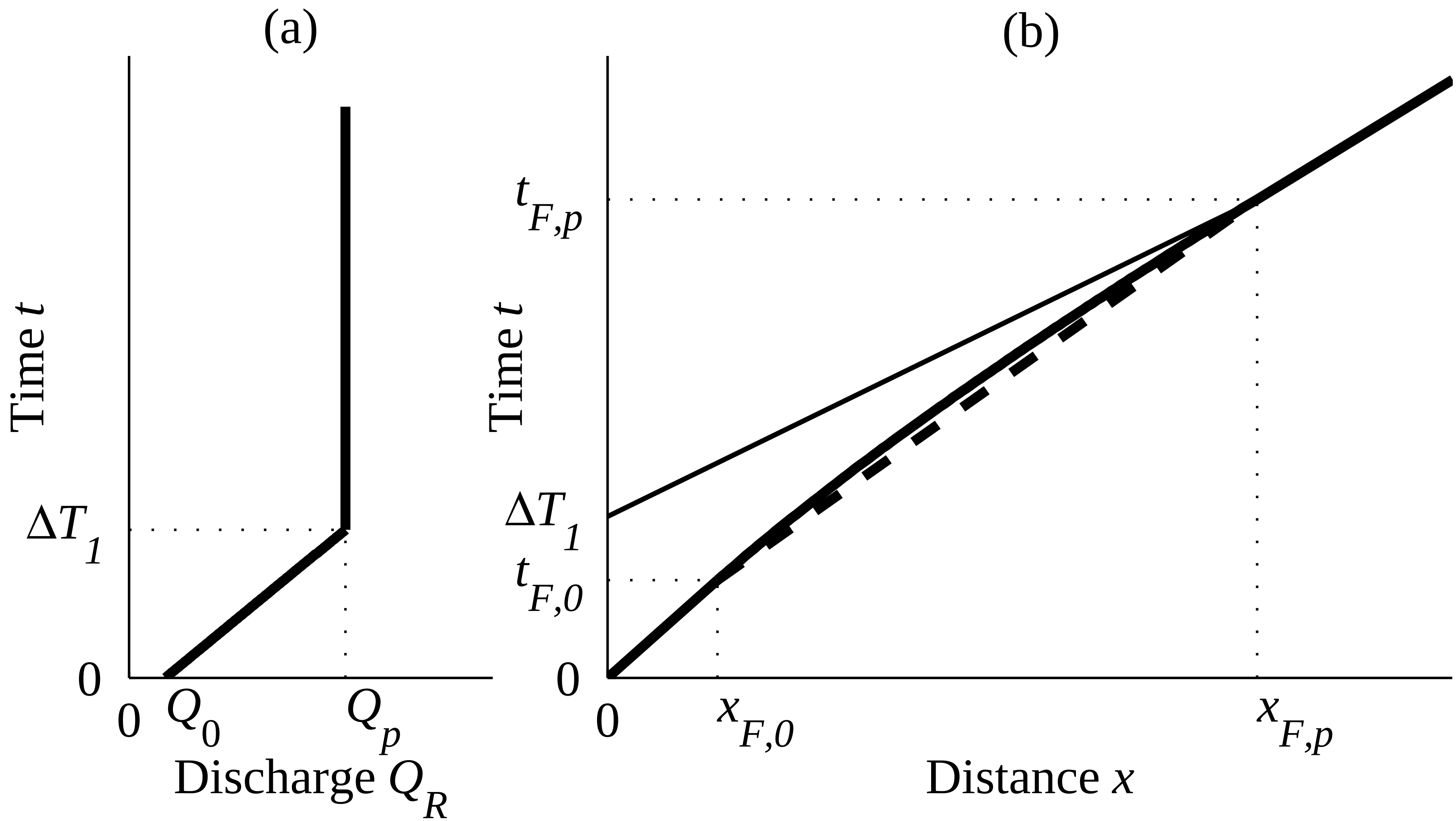

Figure 7

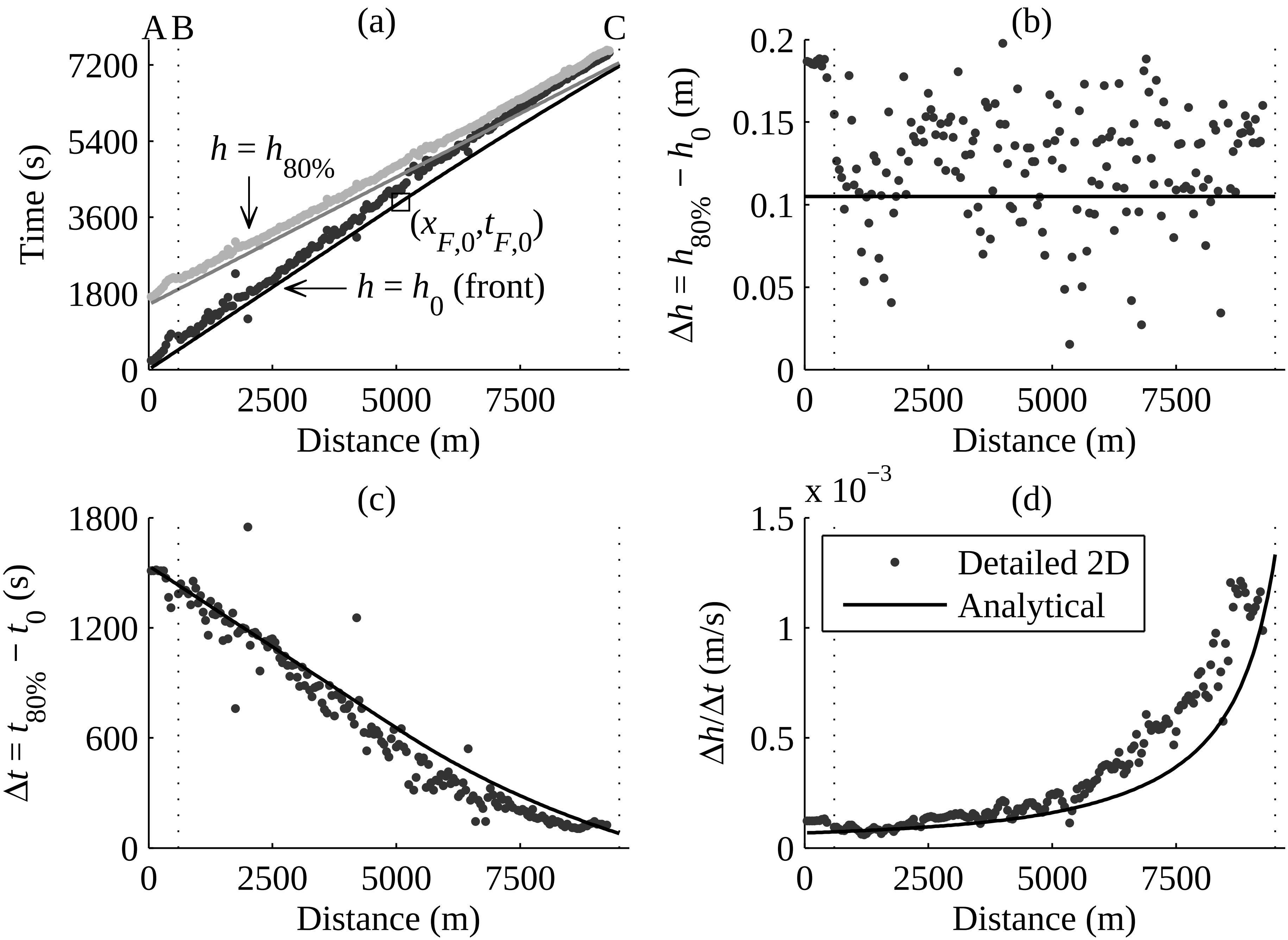

(a)
A B
C
7200
5400
3600
1800
0
Time (s)
h = h80%
(xF,0,tF,0)
h = h0 (front)
0
2500
5000
7500
Distance (m)
(b)
0.2
0.15
0.1
0.05
0
Δh = h80% − h0 (m)
Distance (m)
(c)
1800
1200
600
0
Δt = t80% − t0 (s)
Distance (m)
x 10−3
(d)
1.5
1
0.5
0
Detailed 2D
Analytical
Δh/Δt (m/s)
Distance (m)

Figure 8

Click here to download Figure fig8.eps

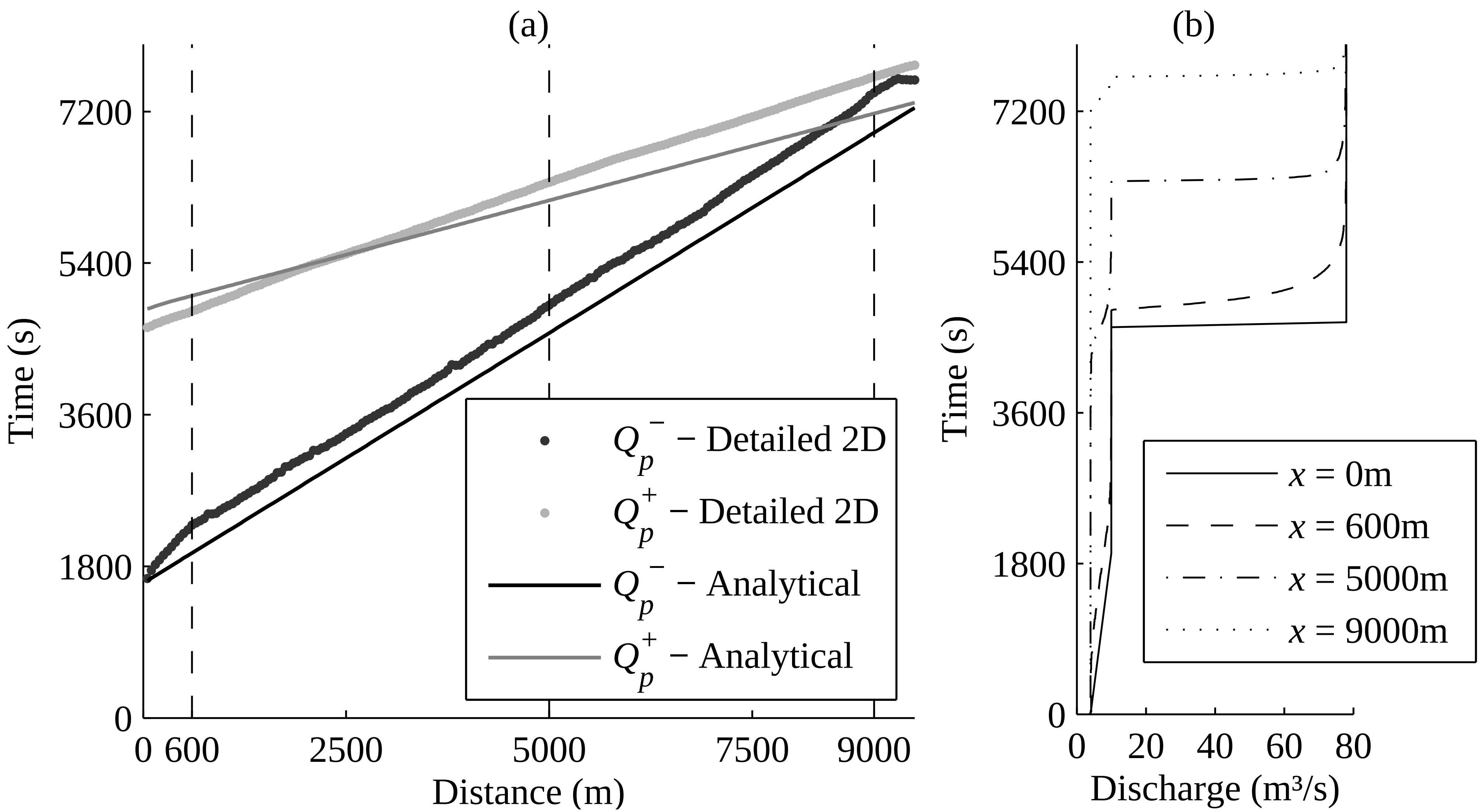

Figure 9

Click here to download Figure fig9.eps

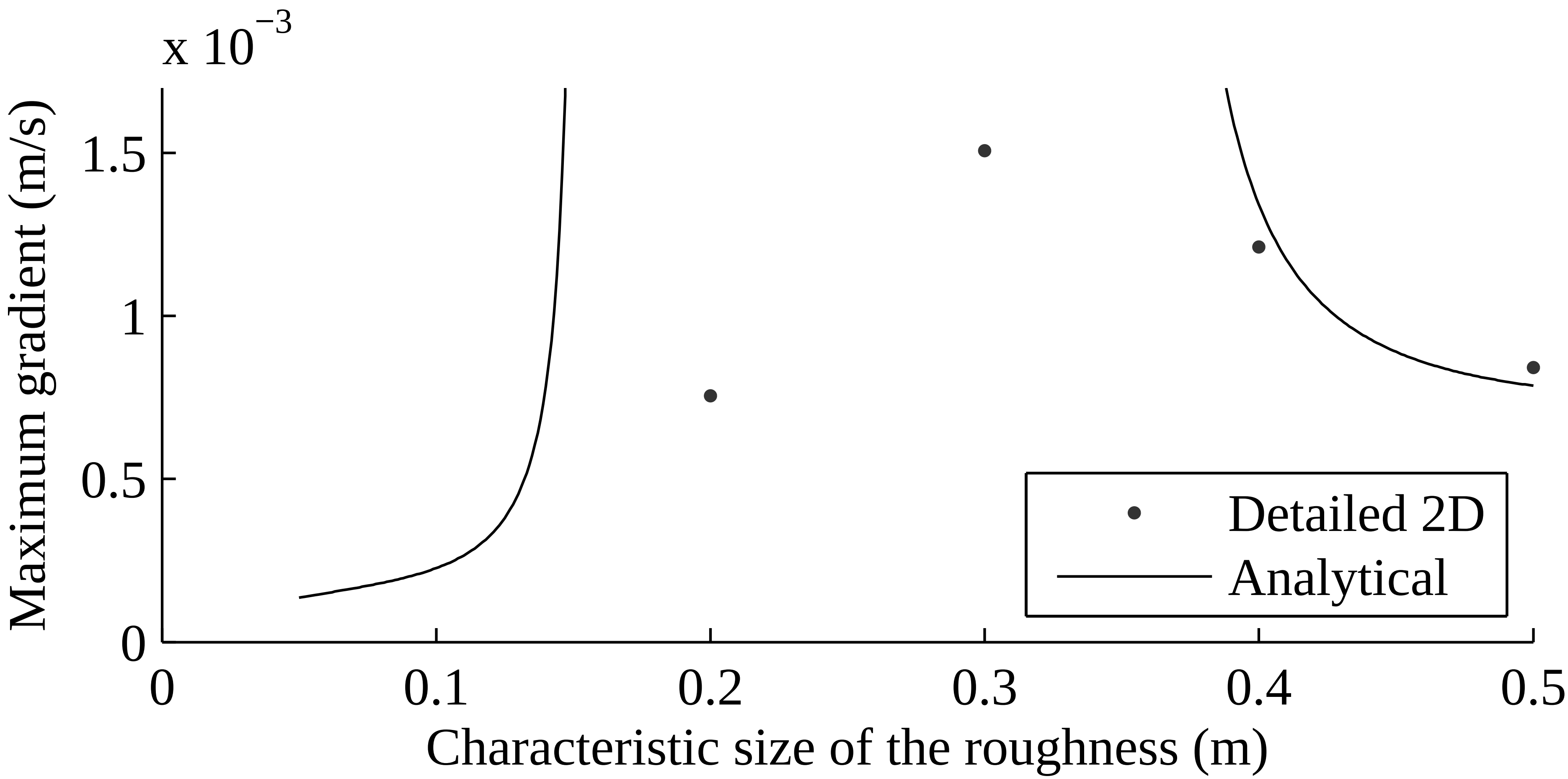

Figure 10

Click here to download Figure fig10.eps